

A self-aligning end-effector robot for individual joint training of the human arm

Sivakumar Balasubramanian¹ , Sandeep Guguloth²,
Javeed Shaikh Mohammed²  and S Sujatha²

Abstract

Aim: Intense training of arm movements using robotic devices can help reduce impairments in stroke. Recent evidence indicates that independent training of individual joints of the arm with robots can be as effective as coordinated multi-joint arm training. This makes a case for designing and developing robots made for training individual joints, which can be simpler and more compact than the ones for coordinate multi-joint arm training. The design of such a robot is the aim of the work presented in this paper.

Methods: An end-effector robot kinematic design was developed and the optimal robot link lengths were estimated using an optimization procedure. A simple algorithm for automatically detecting human limb parameters is proposed and its performance was evaluated through a simulation study.

Results: A six-degrees-of-freedom end-effector robot with three actuated degrees-of-freedom and three non-actuated self-aligning degrees-of-freedom for safe assisted training of the individual joints (shoulder or elbow) of the human arm was conceived. The proposed robot has relaxed constraints on the relative positioning of the human limb with respect to the robot. The optimized link lengths chosen for the robot allow it to cover about 80% of the human limb's workspace, and possess good overall manipulability. The simple estimation procedure was demonstrated to estimate human limb parameters with low bias and variance.

Discussion: The proposed robot with three actuated and three non-actuated degrees-of-freedom has a compact structure suitable for both the left and right arms without any change to its structure. The proposed automatic estimation procedure allows the robot to safely apply forces and impose movements to the human limb, without the need for any manual measurements. Such compact robots have the highest potential for clinical translation.

Keywords

Arm, rehabilitation, robotics, mechanisms, self-aligning

Date received: 12 July 2020; accepted: 12 April 2021

Introduction

Robot-assisted rehabilitation of arm function, in chronic stroke patients, has been found to be as effective as intensity matched conventional therapy for reducing impairments.^{1–3} However, the growing demand for rehabilitation services cannot be met through one-on-one therapist-administered intense training protocols. Technological tools that improve access, and efficiently deliver such services are vital for establishing sustainable service and care pathways. Robots are one such technology that can physically interact with participants to allow graded intense training of various sensorimotor functions. However, the infiltration of robots into routine clinical practice has been poor. This is primarily due to their high cost-to-benefit ratio, limited features, and bulky nature,

especially in the case of arm robots. There is a need for fresh approaches to designing arm rehabilitation robots that can address some of their current shortcomings to improve their potential for commercial translation and eventual clinical acceptance.

¹Department of Bioengineering, Christian Medical College, Vellore, India

²Department of Mechanical Engineering, Indian Institute of Technology – Madras, Chennai, India

Corresponding authors:

Sivakumar Balasubramanian, Department of Bioengineering, Christian Medical College, Vellore, Tamil Nadu 632002, India.
Email: siva82kb@cmcvellore.ac.in

Sujatha Srinivasan, Department of Mechanical Engineering, Indian Institute of Technology – Madras, Chennai, Tamil Nadu 600036, India.
Email: sujsree@iitm.ac.in



This work presents a different approach toward robot-assisted arm rehabilitation focusing on individual joint training, unlike most existing arm robots that are designed for coordinated multi-joint arm training.

There is some evidence in the current literature supporting the hypothesis that individual joint training is not inferior to coordinated multi-joint training. A study by Milot et al. used the BONES robot to administer multi-joint and single-joint training in moderately impaired chronic stroke participants, and found that both groups showed improvements in both motor function and impairments.⁴ Interestingly, they did not find the multi-joint training to be superior to the single-joint training approach. Although only a pilot study with 20 participants, this finding is also supported by other evidence in the literature. Schaefer et al. found that training on a single activity of daily living (ADL) generalized to untrained tasks in chronic stroke participants.⁵ The study by Fluet et al. investigating robot-assisted upper limb (UL) training showed that training the arm and hand together as a functional unit was no different from training the arm and hand separately.⁶ A study on healthy individuals by Klein et al. found that individual training of parts of a complex movement resulted in slightly better learning and retention.⁷ These results support the idea of developing a simple, compact, and cost-effective robot for training individual joints, rather than developing one for coordinated multi-joint arm movements. This is the primary objective of the current work, which focuses on the development of a robot for assisted training of two degrees-of-freedom (*dof*) of the shoulder or elbow joint.

Although *exoskeleton* robots are well suited for supporting and assisting individual joint movements,^{8–13} the strict constraints of alignment of joint axes between the robot and the human can complicate their design and use. On the other hand, *end-effector* robots have structures that are independent of that of the human limb.^{14–17} They have significantly fewer constraints on the location and the orientation of the human joint with respect to the robot, thus making it much easier to interface a human limb with the robot. Given these advantages, we chose to implement an end-effector based approach for the proposed robot for training individual joints.

Conventional end-effector robots for arm rehabilitation are attached to the human limb at the hand, where they apply interaction forces to impose arm movements. Such an approach cannot be used to impose movements at an individual joint of the arm as this human-robot closed kinematic chain¹ is under-constrained. An end-effector robot for training a specific joint will need to be directly attached to the human limb segments that is anatomically connected to the joint of interest (e.g., upper-arm for the shoulder, and forearm for the elbow). In order to ensure that the

robot imposes precise and safe movements and forces/torques to the human limb, it is essential for the robot to be aware of the details of the human limb's kinematic chain and its parameters. Current end-effector robots do not take into consideration the details of the human limb's kinematic chain.

To this end, we present a 6-*dof* end-effector robot AREBO (Arm **R**ehabilitation **R**obot) with three actuated (active) *dof* and three unactuated (passive) *dof*. The current paper focuses on the details of the design of AREBO's kinematic chain, its optimization, and an algorithm for continuously tracking the kinematic parameters of the human limb. AREBO can support and assist two *dof* of a human joint, which we assume as the human shoulder joint for demonstration purposes. We also present a simple approach for automatically estimating and tracking the human limb's kinematic parameters, which will be used to control the interaction of the robot with the human limb.

Design of AREBO's kinematics chain

The objective was to develop a compact, portable robot for training movements of individual joints of the human arm (shoulder and elbow), which can be used for both the left and right arms without requiring any change to the robot's structure. Furthermore, we also wanted to avoid the need for precise positioning and orientation of the patient with respect to the robot, which can be difficult and time consuming with severely affected patients. These design requirements can be fulfilled by an end-effector type robot, the type chosen for designing AREBO.

Consider the human limb with a joint (e.g., shoulder joint) located at the origin of a reference frame \mathcal{H}_0 , depicted in Figure 1, with a rigid body (e.g., upper-arm depicted as a red ellipse) with a reference frame \mathcal{H}_3 attached to it. This rigid body can undergo pure rotational movements with respect to the frame \mathcal{H}_0 . Let \mathcal{R}_0 be an earth-fixed reference frame, which acts as the base of the robot that interfaces to the human limb. We assume that the robot's endpoint is attached rigidly to the origin of \mathcal{H}_3 , which is the point of physical interaction between the robot and the human. The homogenous transformation matrices ${}^{\mathcal{R}_0}\mathbf{H}$ and ${}^{\mathcal{H}_0}\mathbf{H}$ represent the frame \mathcal{H}_0 with respect to \mathcal{R}_0 , and frame \mathcal{H}_3 with respect to \mathcal{H}_0 , respectively.

$$\begin{aligned} {}^{\mathcal{R}_0}\mathbf{H} &= \begin{bmatrix} {}^{\mathcal{R}_0}\mathbf{R} & {}^{\mathcal{R}_0}\mathbf{p}_{\mathcal{H}_0} \\ \mathbf{0} & 1 \end{bmatrix} & {}^{\mathcal{H}_0}\mathbf{H} &= \begin{bmatrix} {}^{\mathcal{H}_0}\mathbf{R} & {}^{\mathcal{H}_0}\mathbf{p}_{\mathcal{H}_3} \\ \mathbf{0} & 1 \end{bmatrix} \\ {}^{\mathcal{R}_0}{}_{\mathcal{H}_0}\mathbf{R} &= \begin{bmatrix} {}^{\mathcal{R}_0}\mathbf{x}_{\mathcal{H}_0} & {}^{\mathcal{R}_0}\mathbf{y}_{\mathcal{H}_0} & {}^{\mathcal{R}_0}\mathbf{z}_{\mathcal{H}_0} \end{bmatrix} \\ {}^{\mathcal{H}_0}{}_{\mathcal{H}_3}\mathbf{R} &= \begin{bmatrix} {}^{\mathcal{H}_0}\mathbf{x}_{\mathcal{H}_3} & {}^{\mathcal{H}_0}\mathbf{y}_{\mathcal{H}_3} & {}^{\mathcal{H}_0}\mathbf{z}_{\mathcal{H}_3} \end{bmatrix} \end{aligned}$$

where, ${}^{\mathcal{A}}\mathbf{B}\mathbf{R}$ is the rotation matrix representing frame \mathcal{B} with respect to \mathcal{A} , and ${}^{\mathcal{A}}\mathbf{p}_{\mathcal{B}}$ is the location of the origin

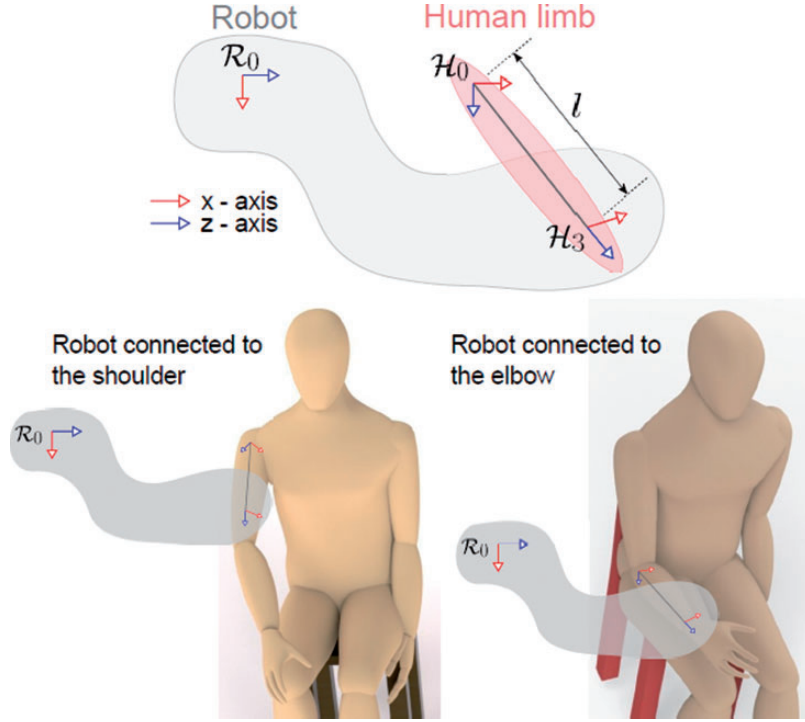


Figure 1. Depiction of a human-robot closed-loop kinematic chain where the movements of the human limb are to be assisted by the robot.

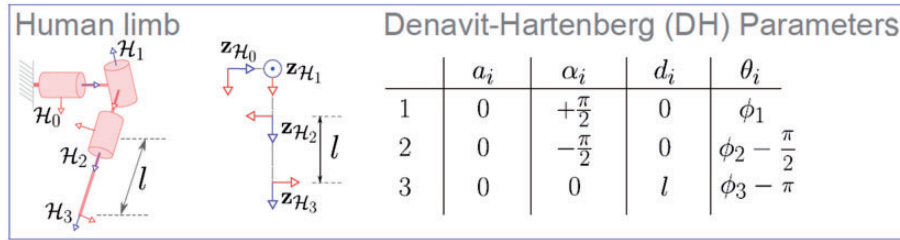


Figure 2. Details of the human limb's kinematic chain. The human limb considered in this work is a two or three *dof* chain with the structure shown in the figure. The third *dof* is optional.

of frame \mathcal{B} represented with respect to the origin of frame \mathcal{A} , represented in frame \mathcal{A} .

To simplify the process of connecting the robot to a human limb, the robot must not strictly constrain the location and orientation of the human limb with respect to the robot, i.e., no strict constraints on ${}^{\mathcal{R}_0}\mathbf{H}$. Additionally, the robot must also accommodate human limbs of different sizes, i.e., variations in l between different participants (Figure 1).

Human limb's kinematic chain

We assume the human shoulder joint at \mathcal{H}_0 to be a spherical joint realized as three intersecting orthogonal revolute joints (Figure 2) with generalized coordinates $\phi(t) = [\phi_1(t) \ \phi_2(t) \ \phi_3(t)]^\top$, where $\phi_1(t)$ and $\phi_2(t)$ are the shoulder flexion/extension and shoulder abduction/adduction angles, respectively, at time t .

The Denavit-Hartenberg (DH) parameters for the human limb are shown in Figure 2. The position and orientation of \mathcal{H}_3 with respect to \mathcal{H}_0 is given by,

$${}^{\mathcal{H}_0}\mathbf{H}(\phi) = \begin{bmatrix} {}^{\mathcal{H}_0}\mathbf{R}(\phi) & {}^{\mathcal{H}_0}\mathbf{p}_{\mathcal{H}_3}(\phi) \\ \mathbf{0} & 1 \end{bmatrix}$$

$${}^{\mathcal{H}_0}\mathbf{R}(\phi) = \begin{bmatrix} \tilde{s}_1\tilde{s}_3 - \tilde{c}_1\tilde{s}_2\tilde{c}_3 & \tilde{s}_1\tilde{c}_3 + \tilde{c}_1\tilde{s}_2\tilde{s}_3 & \tilde{c}_1\tilde{c}_2 \\ -\tilde{s}_1\tilde{s}_2\tilde{c}_3 - \tilde{c}_1\tilde{s}_3 & \tilde{s}_1\tilde{s}_2\tilde{s}_3 - \tilde{c}_1\tilde{c}_3 & \tilde{s}_1\tilde{c}_2 \\ \tilde{c}_2\tilde{c}_3 & -\tilde{c}_2\tilde{s}_3 & \tilde{s}_2 \end{bmatrix} \quad (1)$$

$${}^{\mathcal{H}_0}\mathbf{p}_{\mathcal{H}_3}(\phi) = \begin{bmatrix} l\tilde{c}_1\tilde{c}_2 \\ l\tilde{s}_1\tilde{c}_2 \\ l\tilde{s}_2 \end{bmatrix}$$

where, $\tilde{s}_{i_1 i_2 \dots i_n} = \sin\left(\sum_{k=1}^n \phi_{i_k}\right)$ and $\tilde{c}_{i_1 i_2 \dots i_n} = \cos\left(\sum_{k=1}^n \phi_{i_k}\right)$.

AREBO'S kinematic chain

We are only interested in assisting the shoulder flexion/extension and shoulder abduction/adduction movements of the shoulder joint with the robot in the current application. This movement assistance can be accomplished by applying forces orthogonal to $\mathbf{z}_{\mathcal{H}_3}$, which will result in pure moments about $\mathbf{z}_{\mathcal{H}_0}$ and $\mathbf{z}_{\mathcal{H}_1}$, and ensure there are no forces along the length of the human limb that push it into or pull it away from the shoulder joint.¹⁸ This feature requires the robot to possess the following capabilities:

1. It must **apply forces in any arbitrary direction** in space with respect to \mathcal{R}_0 . Thus, ensuring it can apply forces orthogonal to $\mathbf{z}_{\mathcal{H}_3}$, which can have an arbitrary direction depending on the location of the shoulder joint and the joint configuration of the human limb.
2. The robot needs precise **measurement of the orientation of ${}^{\mathcal{R}_0}\mathbf{z}_{\mathcal{H}_3}$** to be able to apply forces orthogonal to ${}^{\mathcal{R}_0}\mathbf{z}_{\mathcal{H}_3}$.
3. The robot must **align to any arbitrary orientation of \mathcal{H}_3 with respect to \mathcal{R}_0** , to prevent applying unwanted moments at the interface between the human limb and the robot.

An appropriately designed 6-*dof* robot can achieve any arbitrary position and orientation within its workspace. To apply a force in any arbitrary direction at the robot's endpoint in 3 D space, we need at least three actuated *dof* for the robot. The remaining three *dof* can be unactuated, allowing them to self-align to any arbitrary orientation of the human limb \mathcal{H}_3 . A schematic of the current design for AREBO's kinematic chain is shown in Figure 3, which has 6 revolute joints arranged in the specific order shown in the figure. The robot's generalized coordinates are represented by $\boldsymbol{\theta}(t) = [\theta_1(t) \ \theta_2(t) \ \dots \ \theta_6(t)]^\top$, where $\theta_i(t) \in [0, 2\pi)$ is the generalized coordinate corresponding to the i th revolute joint in Figure 3. The position and orientation of the robot's endpoint frame \mathcal{R}_6 , represented by ${}^{\mathcal{R}_0}\mathbf{H}$ depends on $\boldsymbol{\theta}(t)$. The DH parameters of AREBO's

proposed kinematic structure is also listed in a table in Figure 3; the three parameters r_1 , r_2 , and r_3 are the different robot link lengths. The resulting homogenous transformation matrix representing \mathcal{R}_6 in \mathcal{R}_0 is as follows,

$${}^{\mathcal{R}_0}\mathbf{H}(\boldsymbol{\theta}) = \begin{bmatrix} {}^{\mathcal{R}_0}\mathbf{R}(\boldsymbol{\theta}) & {}^{\mathcal{R}_0}\mathbf{p}_{\mathcal{R}_6}(\boldsymbol{\theta}) \\ \mathbf{0} & 1 \end{bmatrix}$$

$${}^{\mathcal{R}_0}\mathbf{R}(\boldsymbol{\theta}) = \begin{bmatrix} c_1 & 0 & s_1 \\ s_1 & 0 & -c_1 \\ 0 & 1 & 0 \end{bmatrix}$$

$$\times \begin{bmatrix} s_{234}s_5s_6 + c_{234}c_6 & s_{234}s_5c_6 - c_{234}s_6 & s_{234}c_5 \\ -c_{234}s_5s_6 + s_{234}c_6 & -c_{234}s_5c_6 - s_{234}s_6 & -c_{234}c_5 \\ s_6c_5 & c_5c_6 & -s_5 \end{bmatrix}$$

$${}^{\mathcal{R}_0}\mathbf{p}_{\mathcal{R}_6}(\boldsymbol{\theta}) = \begin{bmatrix} (r_1c_2 + r_2c_{23} + r_3c_{234})c_1 \\ (r_1c_2 + r_2c_{23} + r_3c_{234})s_1 \\ r_1s_2 + r_2s_{23} + r_3s_{234} \end{bmatrix} \quad (2)$$

where, $s_{i_1i_2\dots i_n} = \sin\left(\sum_{k=1}^n \theta_{i_k}\right)$ and $c_{i_1i_2\dots i_n} = \cos\left(\sum_{k=1}^n \theta_{i_k}\right)$.

Human-robot closed kinematic chain

A closed-loop kinematic chain is formed when AREBO is connected to the human limb, such that the frames \mathcal{R}_6 and \mathcal{H}_3 match in position and orientation.

$${}^{\mathcal{R}_0}\mathbf{H}(\boldsymbol{\theta}) = {}^{\mathcal{R}_0}\mathbf{H}(\boldsymbol{\phi}) = {}^{\mathcal{R}_0}\mathbf{H} \cdot {}^{\mathcal{H}_0}\mathbf{H}(\boldsymbol{\phi}) \quad (3)$$

We assume that the orientation of \mathcal{R}_0 and \mathcal{H}_0 are the same, but they are displaced, i.e.,

$${}^{\mathcal{R}_0}\mathbf{H} = \begin{bmatrix} \mathbf{I}_3 & {}^{\mathcal{R}_0}\mathbf{p}_{\mathcal{H}_0} \\ \mathbf{0} & 1 \end{bmatrix} \quad (4)$$

where, \mathbf{I}_3 is a 3×3 identity matrix.

The first three joints of the robot shown in a darker color in Figure 4 are the actuated joints, while the rest three (shown in a lighter shade) are unactuated. These sections are shown separately in Figure 4 to

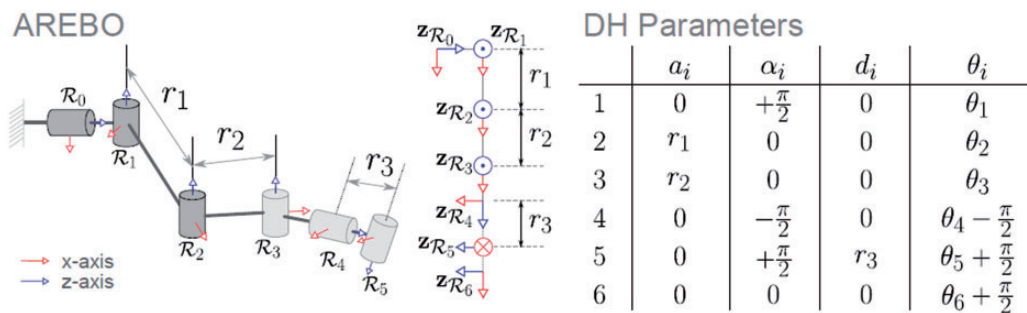


Figure 3. Details of the proposed robot's kinematic chain. The robot has 6 *dof* arranged in the particular manner shown in the figure. This allows the robot to achieve a range of positions and orientations within its reachable workspace. The first three *dof* (shown in dark gray) are actuated, while the rest three *dof* (shown in light gray) are passive self-aligning joints.

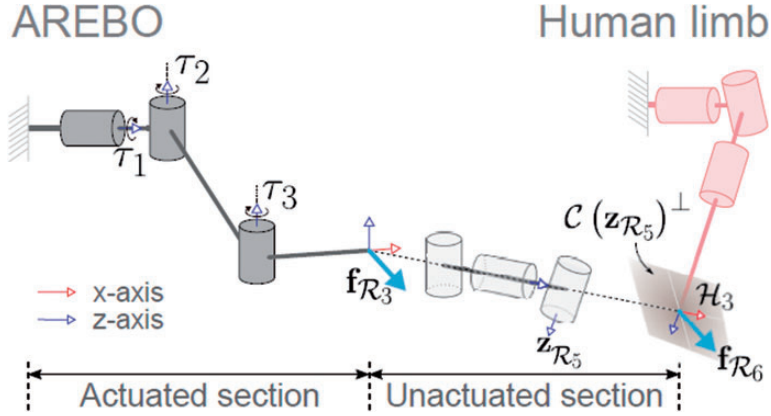


Figure 4. Detailed depiction of the human-robot closed kinematic chain, along with the interaction force applied by the robot on the human limb. The endpoint force $\mathbf{f}_{\mathcal{R}_6}$ on the human limb is determined by the torques acting on the first three actuated *dof*, which need to be appropriately chosen to ensure $\mathbf{f}_{\mathcal{R}_6}$ is orthogonal to $\mathbf{z}_{\mathcal{H}_3}$.

demonstrate the different roles of the two sections. The actuated section is responsible for applying appropriate forces on the human limb, while the unactuated section helps in self-aligning the robot's endpoint \mathcal{R}_6 to the human arm \mathcal{H}_3 . The force resulting from the application of torques τ_1, τ_2, τ_3 at the three actuated robot joints will be transmitted to the human limb through the robot's unactuated section. In order to induce pure moments about the first two joints ($\mathbf{z}_{\mathcal{H}_0}$ and $\mathbf{z}_{\mathcal{H}_1}$ in Figure 4) of the human limb, the robot's endpoint force $\mathbf{f}_{\mathcal{R}_6}$ must be orthogonal to $\mathbf{z}_{\mathcal{H}_3}$.

When the robot and the human limb are connected ($\mathcal{R}_6 = \mathcal{H}_3$), the robot's $\mathbf{x}_{\mathcal{R}_5}, \mathbf{y}_{\mathcal{R}_5}$ are orthogonal to the human limb's $\mathbf{z}_{\mathcal{H}_3}$. Applying torques at the three actuated joints $\mathbf{z}_{\mathcal{R}_0}, \mathbf{z}_{\mathcal{R}_1}$, and $\mathbf{z}_{\mathcal{R}_2}$ will result in a force $\mathbf{f}_{\mathcal{R}_3}$ generated at the origin of \mathcal{R}_3 (Figure 4). This force is transmitted to the human limb through the robot's unactuated section, i.e., $\mathbf{f}_{\mathcal{R}_6} = \mathbf{f}_{\mathcal{R}_3}$, which we would like to be orthogonal to $\mathbf{z}_{\mathcal{R}_3}$, i.e., $\mathbf{f}_{\mathcal{R}_3} = f_x \cdot \mathbf{x}_{\mathcal{R}_5} + f_y \cdot \mathbf{y}_{\mathcal{R}_5} \in \mathcal{C}(\begin{bmatrix} \mathbf{x}_{\mathcal{R}_5} & \mathbf{y}_{\mathcal{R}_5} \end{bmatrix})$, where $f_x, f_y \in \mathbb{R}$; $\mathcal{C}(\begin{bmatrix} \mathbf{x}_{\mathcal{R}_5} & \mathbf{y}_{\mathcal{R}_5} \end{bmatrix})$ is the column space of $\mathbf{x}_{\mathcal{R}_5}$ and $\mathbf{y}_{\mathcal{R}_5}$. The relationship between $\mathbf{f}_{\mathcal{R}_3}$ and the torque $\boldsymbol{\tau} = [\tau_1 \ \tau_2 \ \tau_3]^\top$ is given by the following relationship,

$$\boldsymbol{\tau} = {}^{\mathcal{R}_0}_{\mathcal{R}_3} \mathbf{J}(\boldsymbol{\theta})^\top \mathbf{f}_{\mathcal{R}_3} = {}^{\mathcal{R}_0}_{\mathcal{R}_3} \mathbf{J}(\boldsymbol{\theta})^\top \begin{bmatrix} \mathbf{x}_{\mathcal{R}_5} & \mathbf{y}_{\mathcal{R}_5} \end{bmatrix} \begin{bmatrix} f_x \\ f_y \end{bmatrix} \quad (5)$$

where, ${}^{\mathcal{R}_0}_{\mathcal{R}_3} \mathbf{J}(\boldsymbol{\theta})$ is the Jacobian matrix relating the angular velocities $\dot{\theta}_1(t), \dot{\theta}_2(t), \dot{\theta}_3(t)$ to the linear velocity of the origin of \mathcal{R}_3 . The above equation can be solved for $\boldsymbol{\tau}$ to apply any force $\mathbf{f}_{\mathcal{R}_3}$ that is in the column space of ${}^{\mathcal{R}_0}_{\mathcal{R}_3} \mathbf{J}(\boldsymbol{\theta})$. The Jacobian matrix, $\mathbf{x}_{\mathcal{R}_5}$, and $\mathbf{y}_{\mathcal{R}_5}$ are given by the following,

$${}^{\mathcal{R}_0}_{\mathcal{R}_3} \mathbf{J} = \begin{bmatrix} -(r_1 c_2 + r_2 c_{23}) s_1 & (r_1 c_2 + r_2 c_{23}) c_1 & 0 \\ -(r_1 s_2 + r_2 s_{23}) c_1 & -(r_1 s_2 + r_2 s_{23}) s_1 & r_1 c_2 + r_2 c_{23} \\ -r_2 s_{23} c_1 & -r_2 s_{23} s_1 & r_2 c_{23} \end{bmatrix} \quad (6)$$

$$\mathbf{x}_{\mathcal{R}_5} = \begin{bmatrix} -s_1 c_5 - c_1 s_{234} s_5 \\ -s_1 s_{234} s_5 + c_1 c_5 \\ c_{234} s_5 \end{bmatrix} \quad \mathbf{y}_{\mathcal{R}_5} = \begin{bmatrix} c_1 c_{234} \\ s_1 c_{234} \\ s_{234} \end{bmatrix} \quad (7)$$

Except for the cases where $\theta_3 = n\pi, n \in \mathbb{Z}$, and $(r_1 c_2 + r_2 c_{23}) = 0$, ${}^{\mathcal{R}_0}_{\mathcal{R}_3} \mathbf{J}$ is always full rank and thus any $\mathbf{f}_{\mathcal{R}_3}$ can be applied by appropriately choosing $\boldsymbol{\tau}$.

Identification of human limb parameters

In the human-robot closed kinematic chain, the planning and control of the human limb's movements require information about the location of \mathcal{H}_0 (i.e., ${}^{\mathcal{R}_0} \mathbf{p}_{\mathcal{H}_0}$) and the length of the human limb l . Knowledge of these parameters is crucial for answering the following two specific questions:

1. Can a given desired human limb configuration (ϕ_1, ϕ_2) be reached by the human-robot closed kinematic chain, i.e., $\exists \boldsymbol{\theta}, s.t. {}^{\mathcal{R}_0}_{\mathcal{R}_6} \mathbf{H}(\boldsymbol{\theta}) = {}^{\mathcal{R}_0}_{\mathcal{H}_3} \mathbf{H}(\phi)$?
2. For any reachable human limb configuration (ϕ_1, ϕ_2) , what is the corresponding robot configuration $\boldsymbol{\theta}$ that allows the human limb to achieve (ϕ_1, ϕ_2) ?

Assuming that we know ${}^{\mathcal{R}_0} \mathbf{p}_{\mathcal{H}_0}$ and l , we can answer the two questions by first performing forward kinematics for the human limb to compute ${}^{\mathcal{R}_0}_{\mathcal{H}_3} \mathbf{H}(\phi)$ for a given (ϕ_1, ϕ_2) ; we assume ϕ_3 to be anything as any rotation about this *dof* is accommodated by θ_6 . We then perform inverse kinematics for the robot by assuming ${}^{\mathcal{R}_0}_{\mathcal{R}_6} \mathbf{H}(\boldsymbol{\theta}) = {}^{\mathcal{R}_0}_{\mathcal{H}_3} \mathbf{H}(\phi)$. The algorithm for performing inverse kinematics for AREBO is detailed in online Appendix A. If we obtain a valid $\boldsymbol{\theta}$ for a given (ϕ_1, ϕ_2) , then this human limb configuration is achievable and $\boldsymbol{\theta}$ is the corresponding robot joint configuration.

Given that AREBO allows some freedom for the user to sit with respect to the robot (Figure 7) and can accommodate upper-limbs of different sizes, the values of ${}^{\mathcal{R}_0}\mathbf{p}_{\mathcal{H}_0}$ and l will be different for different users. It is not practical to measure these parameters for each user in order to use the robot. To address this issue, we propose a simple calibration procedure that can automatically estimate these parameters once a user is connected to the robot. This calibration can be done through a least squares estimation procedure, where the robot imposes random, safe movements to the human limb while recording the θ of the robot, and the *pitch* (ϕ_1) and *yaw* (ϕ_2) angles of the human limb. Let us assume that we have a record of the robot and human limb angles.

$$\theta[n] = \{\theta_1[n], \theta_2[n], \dots, \theta_6[n]\}_{n=0}^{N-1}$$

$$\text{and } \phi[n] = \{\phi_1[n], \phi_2[n], \phi_3[n]\}_{n=0}^{N-1}$$

where, $n \in \mathbb{Z}$ is the time index, and $N \in \mathbb{Z}$, $N > 0$ is the length of data available. In the human-robot closed kinematic chain, we have

$${}^{\mathcal{R}_0}\mathbf{p}_{\mathcal{R}_6} = \begin{bmatrix} {}^{\mathcal{R}_0}\mathbf{R} & {}^{\mathcal{R}_0}\mathbf{p}_{\mathcal{H}_0} \\ \mathbf{0} & 1 \end{bmatrix} \begin{bmatrix} {}^{\mathcal{H}_0}\mathbf{p}_{\mathcal{H}_3} \\ 1 \end{bmatrix} = {}^{\mathcal{R}_0}\mathbf{R} \cdot {}^{\mathcal{H}_0}\mathbf{p}_{\mathcal{H}_3} + {}^{\mathcal{R}_0}\mathbf{p}_{\mathcal{H}_0}$$

We have assumed earlier that ${}^{\mathcal{R}_0}\mathbf{R} = \mathbf{I}_3$, and let ${}^{\mathcal{R}_0}\mathbf{p}_{\mathcal{H}_0} = [p_x \ p_y \ p_z]^\top = \mathbf{p}$. Then, for any time instant n we have from the above equation, equations (2) and (1)

$$\begin{aligned} (r_1 c_2[n] + r_2 c_{23}[n] + r_3 c_{234}[n])c_1[n] &= l\tilde{c}_1[n]\tilde{c}_2[n] + p_x \\ (r_1 c_2[n] + r_2 c_{23}[n] + r_3 c_{234}[n])s_1[n] &= l\tilde{s}_1[n]\tilde{c}_2[n] + p_y \\ r_1 s_2[n] + r_2 s_{23}[n] - r_3 s_{234}[n] &= l\tilde{s}_2[n] + p_z \end{aligned} \quad (8)$$

The unknowns in the above equation are p_x, p_y, p_z , and l . We can rewrite the above equation in the following form,

$$\begin{aligned} \begin{bmatrix} \tilde{c}_1[n]\tilde{c}_2[n] & 1 & 0 & 0 \\ \tilde{s}_1[n]\tilde{c}_2[n] & 0 & 1 & 0 \\ \tilde{s}_2[n] & 0 & 0 & 1 \end{bmatrix} \begin{bmatrix} l \\ p_x \\ p_y \\ p_z \end{bmatrix} \\ = \begin{bmatrix} (r_1 c_2[n] + r_2 c_{23}[n] + r_3 c_{234}[n])c_1[n] \\ (r_1 c_2[n] + r_2 c_{23}[n] + r_3 c_{234}[n])s_1[n] \\ r_1 s_2[n] + r_2 s_{23}[n] + r_3 s_{234}[n] \end{bmatrix} \\ [\mathbf{a}[n] \quad \mathbf{I}_3] \begin{bmatrix} l \\ \mathbf{p} \end{bmatrix} = \mathbf{b}[n] \end{aligned} \quad (9)$$

Combining the equations for all n ,

$$\begin{bmatrix} \mathbf{a}[0] & \mathbf{I}_3 \\ \mathbf{a}[1] & \mathbf{I}_3 \\ \vdots & \vdots \\ \mathbf{a}[N-1] & \mathbf{I}_3 \end{bmatrix} \begin{bmatrix} l \\ \mathbf{p} \end{bmatrix} = \begin{bmatrix} \mathbf{b}[0] \\ \mathbf{b}[1] \\ \vdots \\ \mathbf{b}[N-1] \end{bmatrix} \Rightarrow \mathbf{A}\mathbf{v} = \mathbf{A} \begin{bmatrix} l \\ \mathbf{p} \end{bmatrix} = \tilde{\mathbf{b}} \quad (10)$$

If \mathbf{A} is full rank, the least squares estimate of the parameters are given by,

$$\hat{\mathbf{v}} = \begin{bmatrix} \hat{l} \\ \hat{\mathbf{p}} \end{bmatrix} = \begin{bmatrix} \hat{l} \\ \hat{p}_x \\ \hat{p}_y \\ \hat{p}_z \end{bmatrix} = (\mathbf{A}^\top \mathbf{A})^{-1} \mathbf{A}^\top \cdot \tilde{\mathbf{b}} \quad (11)$$

Methods

In this section, we describe the optimization of the robot link length parameters and the simulation analysis of the algorithm for estimating human limb parameters.

The first step in the physical realization of AREBO is the choice of its link lengths r_1, r_2 , and r_3 . These link lengths will determine the robot's workspace and its overall manipulability. The individual endpoint workspaces of the robot $W_{\mathcal{R}}$ and the human limb $W_{\mathcal{H}}$ are given by the following,

$$\begin{aligned} W_{\mathcal{R}} &= \left\{ {}^{\mathcal{R}_0}\mathbf{H}(\theta) \mid \theta \in J_{\mathcal{R}} \subset [0, 2\pi]^6 \right\} \\ W_{\mathcal{H}} &= \left\{ {}^{\mathcal{R}_0}\mathbf{H}(\phi) \mid \phi \in J_{\mathcal{H}} \subset [0, 2\pi]^3 \right\} \end{aligned} \quad (12)$$

where, $J_{\mathcal{R}}$ and $J_{\mathcal{H}}$ are the set of all joint configurations that can be achieved by the robot and the human limb, respectively. $W_{\mathcal{R}}$ and $W_{\mathcal{H}}$ are the set of all endpoint positions and orientations of the robot and the human limb. Here, all positions and orientations are represented with respect to the common frame \mathcal{R}_0 .

When the endpoints of the human limb and robot are attached together, i.e., $\mathcal{R}_6 = \mathcal{H}_3$, the only possible joint configurations $J_{\mathcal{H}}^a$ and $J_{\mathcal{R}}^a$ for the human limb and the robot are those corresponding to the set $W^a = W_{\mathcal{R}} \cap W_{\mathcal{H}_3}$, i.e., $W^a = \left\{ {}^{\mathcal{R}_0}\mathbf{H}(\phi) \mid \phi \in J_{\mathcal{H}}^a \right\} = \left\{ {}^{\mathcal{R}_0}\mathbf{H}(\theta) \mid \theta \in J_{\mathcal{R}}^a \right\}$. In general there will be a reduction in the human limb's workspace $W^a \subseteq W_{\mathcal{H}}$ or $J_{\mathcal{H}}^a \subseteq J_{\mathcal{H}}$. The size of the set W^a is determined by several factors: (i) length of the robot links r_1, r_2 , and r_3 ; (ii) length of

the human limb l ; and (iii) position of the human limb with respect to the robot ${}^{\mathcal{R}_0}\mathbf{p}_{\mathcal{H}_0} = [p_x \ p_y \ p_z]^\top = \mathbf{p}$.

We wish to allow a range of possible values for the parameters l and \mathbf{p} to support the movements of human limbs of different lengths without placing strict constraints on the seating of a participant with respect to the robot. Thus, for given reasonable parameter ranges for l and \mathbf{p} , we would like to choose the robot link lengths to achieve two objectives:

1. Maximize W^a (or $J_{\mathcal{H}}^a$) to minimize the restrictions on the human limb's movement, and
2. Maximize the ability of the robot to apply forces orthogonal to the human limb.

These two objectives can be combined into a single objective function $O(\mathbf{r})$ of the robot link length $\mathbf{r} = [r_1 \ r_2 \ r_3]^\top$,

$$O(\mathbf{r}) = w_1 O_1(\mathbf{r}) + w_2 O_2(\mathbf{r}) \quad (13)$$

where, $O_1(\mathbf{r})$ is a function of W^a , and $O_2(\mathbf{r})$ is a function of the robot's ability to apply forces in the appropriate directions, $0 < w_1, w_2 \in \mathbb{R}$ are the weights for the two objectives. It should be noted that $O_1(\cdot)$ and $O_2(\cdot)$ are only functions of \mathbf{r} as these are obtained by averaging these measures across the different possible values of l and \mathbf{p} . The optimal value for the robot's link lengths \mathbf{r}^{opt} is obtained by maximizing $O(\mathbf{r})$ for a given range of values for l and \mathbf{p} .

Human limb's workspace $O_1(\mathbf{r})$: The first objective function $O_1(\mathbf{r})$ depends on the human limb's workspace when it is connected to a robot with link lengths \mathbf{r} . We chose to quantify the size of the workspace in the joint space $J_{\mathcal{H}}^a$, where $J_{\mathcal{H}}^a = \{\phi_1, \phi_2, \phi_3\}$. For a given value of \mathbf{r} , l , and \mathbf{p} , we quantify the normalized workspace of the human limb as the following,

$$\eta_1(\mathbf{r}, l, \mathbf{p}) = \frac{\nu(J_{\mathcal{H}}^a)}{\nu(J_{\mathcal{H}})}$$

where, $\nu(\cdot)$ computes the volume of a given set, which implies that $0 \leq \eta_1(\mathbf{r}, l, \mathbf{p}) \leq 1$. $O_1(\mathbf{r})$ is obtained for a given value of \mathbf{r} by computing the average value of $\eta_1(\mathbf{r}, l, \mathbf{p})$ over the range of values for l and \mathbf{p} ,

$$O_1(\mathbf{r}) = \frac{1}{K_l \cdot K_{\mathbf{p}}} \int_l \int_{\mathbf{p}} \eta_1(\mathbf{r}, l, \mathbf{p}) d\mathbf{p} dl \quad (14)$$

where, $K_l = \int_l dl$ and $K_{\mathbf{p}} = \int_{\mathbf{p}} d\mathbf{p}$ are the sizes of sets of parameters l and \mathbf{p} , respectively.

Robot manipulability $O_2(\mathbf{r})$: Manipulability provides a measure of how easily a robot can apply forces in

different directions, which, in general, depends on the robot's joint configuration. In the current application, we are not interested in applying forces in any direction, but only in the plane orthogonal to the human limb. In the closed kinematic chain shown in Figure 4, for a given \mathbf{r} , l , and \mathbf{p} , and for any human limb configuration in $\phi \in J_{\mathcal{H}}^a$, there is a corresponding point $\theta \in J_{\mathcal{R}}^a$. The relationship between the torque τ at the robot's joints and its endpoint force $\mathbf{f}_{\mathcal{R}_6}$ depends on the robot's Jacobian matrix for the current joint configuration θ (equation (5)). For any given torque the resulting force along the human limb (\mathbf{f}_z) and orthogonal to the human limb (\mathbf{f}_{xy}) can be obtained from the following expressions,

$$\mathbf{f}_{xy} = \mathbf{P}_{xy}(\theta) \cdot {}^{\mathcal{R}_0}_{\mathcal{R}_3} \mathbf{J}(\theta)^{-\top} \cdot \tau \quad \mathbf{f}_z = \mathbf{P}_z(\theta) \cdot {}^{\mathcal{R}_0}_{\mathcal{R}_3} \mathbf{J}(\theta)^{-\top} \cdot \tau \quad (15)$$

where, $\mathbf{P}_{xy} = \mathbf{x}_{\mathcal{R}_5} \mathbf{x}_{\mathcal{R}_5}^\top + \mathbf{y}_{\mathcal{R}_5} \mathbf{y}_{\mathcal{R}_5}^\top$ and $\mathbf{P}_z = \mathbf{z}_{\mathcal{R}_5} \mathbf{z}_{\mathcal{R}_5}^\top$ are the orthogonal projection matrices on to the xy -plane and the z axis of the frame \mathcal{R}_5 . We would ideally like the robot's kinematic chain to be inherently more suited to apply forces in the xy -plane of \mathcal{R}_5 , rather than the z -axis, for a given τ . This property is captured by the following measure, which captures the ratio of the maximum possible force in the xy -plane with respect to that of the z -axis for a given torque τ .

$$\eta_2(\mathbf{r}, l, \mathbf{p}) = \frac{1}{K_\theta} \int_\theta H(\rho(\theta) - 1) d\theta,$$

$$\rho(\theta) = \frac{\|\mathbf{P}_{xy}(\theta) \cdot {}^{\mathcal{R}_0}_{\mathcal{R}_3} \mathbf{J}(\theta)^{-\top}\|_2}{\|\mathbf{P}_z(\theta) \cdot {}^{\mathcal{R}_0}_{\mathcal{R}_3} \mathbf{J}(\theta)^{-\top}\|_2}, \quad H(x) = \begin{cases} 0, & x < 0 \\ 1, & x \geq 1 \end{cases}$$

where, $K_\theta = \int_\theta d\theta$ is the size of $J_{\mathcal{R}}^a$, $\|\cdot\|_2$ is the induced second norm of a given matrix, and $H(\cdot)$ is the step function. The ratio $\rho(\theta)$ is a measure of the "ease" of applying a force along the xy -plane compared to that of z -axis at the joint configuration θ . Ideally, we would like this ratio to be greater than 1, and thus this ratio is transformed using the step function, such that ratios that are less than 1 are mapped to 0, and the ones greater than or equal to 1 are mapped to 1. Thus, $\eta_2(\mathbf{r}, l, \mathbf{p})$ can be interpreted as the proportion of points in the robot's workspace with the ratio $\rho(\theta) \geq 1$, which implies that $0 \leq \eta_2 \leq 1$.

$O_2(\mathbf{r})$ is obtained from $\eta_2(\cdot)$ by averaging over the other two arguments l , and \mathbf{p} (like equation (14)).

$$O_2(\mathbf{r}) = \frac{1}{K_l \cdot K_{\mathbf{p}}} \int_l \int_{\mathbf{p}} \eta_2(\mathbf{r}, l, \mathbf{p}) d\mathbf{p} dl \quad (16)$$

Table 1. Set of parameter values for the robot and the human limb used for the robot link length optimization program. There are a total of 484 robot parameter sets (r_1, r_2, r_3) that are searched, and for each of these 484 parameter sets the objective functions $O_1(\cdot)$ and $O_2(\cdot)$ are computed by averaging over the 81 different human limb parameters $K_l = 3$, $K_p = 27$.

Parameter	Values (cm)	No. of values
r_1	{20, 21, ... 30}	11
r_2	{10, 11, ... 20}	11
r_3	{12, 13, 14, 15}	4
l	{15, 17.5, 20}	3
p_x, p_y	{-10, 0, 10}	3
p_z	{10, 20, 30}	3

Optimization of robot link lengths

The optimization of the robot link lengths was carried out numerically through a brute force search over a set of parameters values for \mathbf{r} , l , and \mathbf{p} , which are listed in Table 1. The algorithm for the optimization procedure is as follows,

1. Choose values for the robot link lengths: $\tilde{\mathbf{r}} = [\tilde{r}_1 \ \tilde{r}_2 \ \tilde{r}_3]^\top$.
2. Choose values for the human limb length and location: \tilde{l} and $\tilde{\mathbf{p}}$.
3. Compute the set of all possible joint configurations for the human limb $J_{\mathcal{H}}^a$ and the robot $J_{\mathcal{R}}^a$ for the chosen robot and human limb parameters.
4. Compute the workspace $\eta_1(\tilde{\mathbf{r}}, \tilde{l}, \tilde{\mathbf{p}})$ and robot manipulability measures $\eta_2(\tilde{\mathbf{r}}, \tilde{l}, \tilde{\mathbf{p}})$.
5. If all possible human limb parameters have been searched, then go to Step 6, else go to Step 2.
6. Compute the two objective functions $O_1(\tilde{\mathbf{r}})$ and $O_2(\tilde{\mathbf{r}})$ from the measures η_1 and η_2 computed for all possible human limb parameters.
7. If all possible robot parameters have been searched, then go to Step 8, else go to Step 1.
8. Find the optimal robot link parameters as the value of the \mathbf{r} that maximizes $O(\mathbf{r})$.

$$\mathbf{r}^{opt} = \arg \max_{\mathbf{r}} (w_1 O_1(\mathbf{r}) + w_2 O_2(\mathbf{r})) \quad (17)$$

We assumed $w_1 = w_2 = 0.5$ for the current optimization problem.

Simulation analysis of human limb parameter estimation

The algorithm for estimating the human limb parameters described in ‘Identification of human limb parameters’ section was evaluated using simulated movement data. Twenty different random parameter sets were

generated from uniform distributions for p_x , p_y , p_z , and l of the human limb.

$$p_x, p_y \sim \mathcal{U}(-10, 10) \quad p_z \sim \mathcal{U}(10, 30) \quad l \sim \mathcal{U}(15, 20)$$

where, $\mathcal{U}(a, b)$ is a uniform probability density function with parameters a and b . The location and length of the human limb were sampled from the same region of parameters used for the optimization problem (Table 1). For each randomly selected parameter set \mathbf{p} and l , 50 different random movements were imposed on the human-robot closed kinematic chain, and the human $\phi[n]$ and robot $\theta[n]$ joint configurations were recorded. The random movements to the human-robot closed chain were achieved by imposing a polysine movement to human joint of the following form,

$$x[n] = \sum_{k=1}^K A_k \sin(2\pi f_k n + \psi_k), \quad 0 \leq n \leq L-1$$

where, K is the number of sinusoidal components and was chosen as 3, $f_k = \{0.2, 0.5, 1.0\}$ Hz, $A_k = \{1.0, 0.5, 0.1\}$, and ψ_k was chosen randomly from a uniform distribution between $-\pi$ and π . The polysine signal $x[n]$ was appropriately scaled to cover a range of 0 deg to 90 deg for ϕ_1 , and -30 deg to 30 deg for ϕ_2 . The simulated data was assumed to be sampled at 100 Hz and 5 s of calibration movements were simulated. Gaussian white noise with two different variances 1deg^2 and 5deg^2 were added to the joint angles to simulate different levels of measurement noise; these two variances were chosen as these were considered to be reasonable noise variances for angles measured with a rotary encoder or a potentiometer. The robot parameters were assumed to be \mathbf{r}^{opt} for these simulations.

The human and robot joint angle data from the simulated calibration procedures were used to estimate the human limb parameters; 50 different estimates for the 20 different sets of human parameters were estimated. The performance of the estimation algorithm was evaluated by computing the distribution of estimation errors for the four parameters.

The code used for robot link length optimization and the analysis of the limb parameter estimation are available for download; refer to online Appendix B for details.

Results

In this section, we present the results from the robot link length optimization and the simulation analysis of the human limb parameter identification algorithm.

Optimization of robot link lengths

The results from the robot link length optimization procedure are shown in Figure 5 in the form of heatmaps as a function of two robot link parameters; the first two rows correspond to the individual objective functions $O_1(\mathbf{r})$ and $O_2(\mathbf{r})$, and the last row corresponds to the overall objective function $O(\mathbf{r})$. The columns display these heatmaps as function of two of the robot link length parameters. As expected, the normalized workspace $O_1(\mathbf{r})$ increases as the robot link lengths increase (first row of Figure 5). On the other hand, the force ratio $O_2(\mathbf{r})$ tends to be higher for shorter link lengths (Figure 5). The overall objective function $O(\mathbf{r})$, which is a weighted sum of $O_1(\mathbf{r})$ and $O_2(\mathbf{r})$ is shown in the third row in Figure 5. Based on this plot and through numerical analysis, the optimal values for the robot link length parameters r_1^{opt} , r_2^{opt} , and r_3^{opt} were found to be 27, 20, and 10 cm, respectively. Out of the 484 ($11 \times 11 \times 4$) robot link lengths searched, the set of robot link parameters that had the top 5% values for the objective function $O(\mathbf{r})$ were found to have r_1 , r_2 , and r_3 in the range 24 – 28 cm, 18 – 20 cm, and 10 cm, respectively. For the optimal link lengths, the range of values for the normalized workspace $\eta_1(\mathbf{r}^{opt}, l, \mathbf{p})$ and normalized force ratio $\eta_2(\mathbf{r}^{opt}, l, \mathbf{p})$ for different values of the human

limb parameters are depicted in Figure 6. The top row shows the normalized workspace, which indicates that \mathbf{r}^{opt} , on average, is able to cover about 80% of the human limb's workspace. The various values of the different parameters appear to result in a similar range of values for the normalized workspace, except for the $p_z = 10$ cm (rightmost figure in the top row in Figure 6), where the normalized workspace is about 60%. Thus, when a participant sits very close to the robot, there is a drop in the participant's workspace. The normalized force ratio (bottom row of Figure 6) appear to be around 0.6–0.7, which means that in general 60–70% of the robot's joint configurations have $\rho(\theta) \geq 1$. Based on the optimal link lengths, a 3D model of the proposed robot is depicted in Figure 7, which shows two scenarios with the robot attached to the upper-arm and the forearm. When it is connected to the upper-arm, the robot can assist shoulder flexion/extension and shoulder abduction/adduction. When it is attached to the forearm, it can support shoulder internal-external rotation and elbow flexion-extension, when the elbow position is constrained.

Identification of human limb parameters

The results from the analysis of the human limb parameter identification procedure are shown in Figure 8.

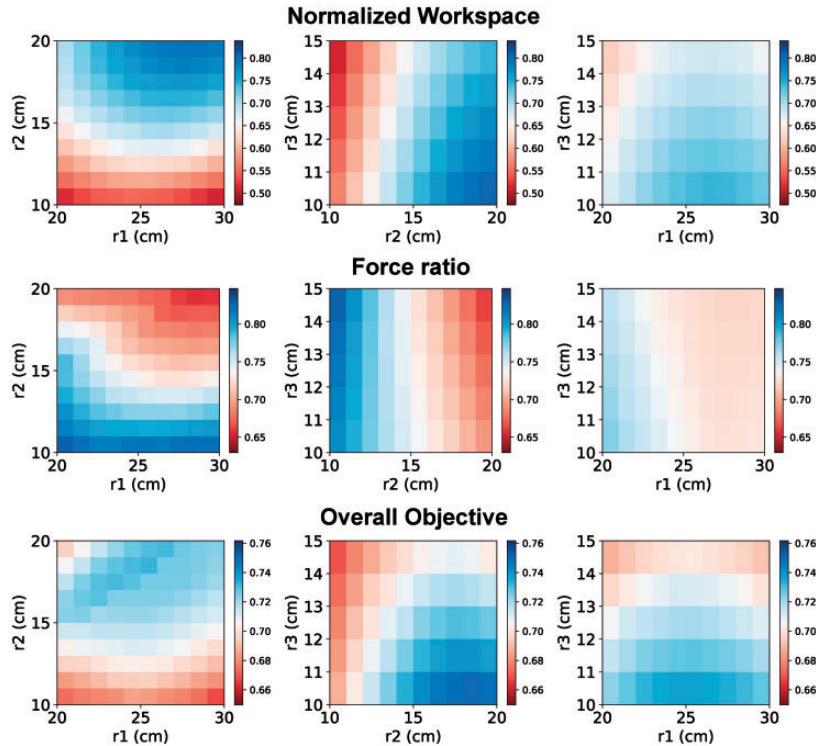


Figure 5. Heatmaps depicting the values of the objective functions O_1 , O_2 and O as a function of the different robot link lengths. These plots show that workspace O_1 and force ratio O_2 are conflicting objectives, and the resulting overall objective that weighs both O_1 and O_2 equally is shown in the bottom row.

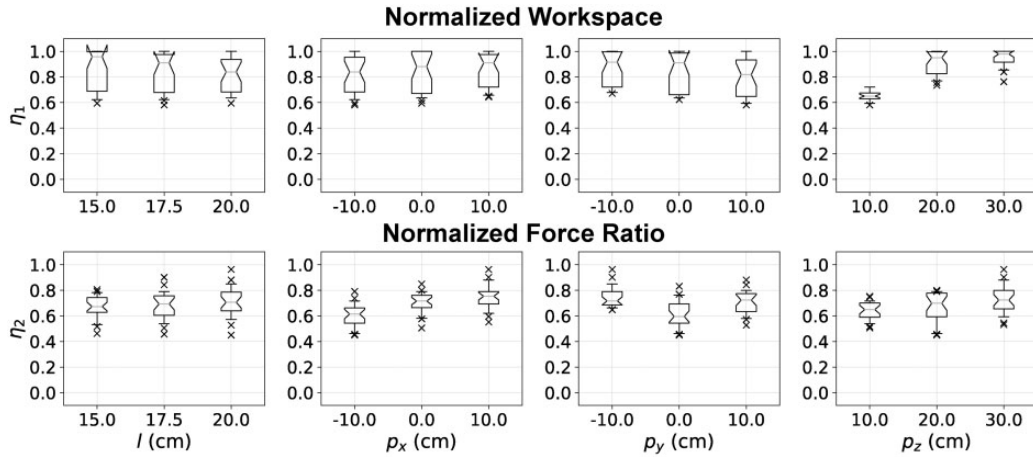


Figure 6. The values of normalized workspace O_1 and force ratio O_2 for the optimal robot link lengths, for the different possible parameters for the human limb (from Table I).

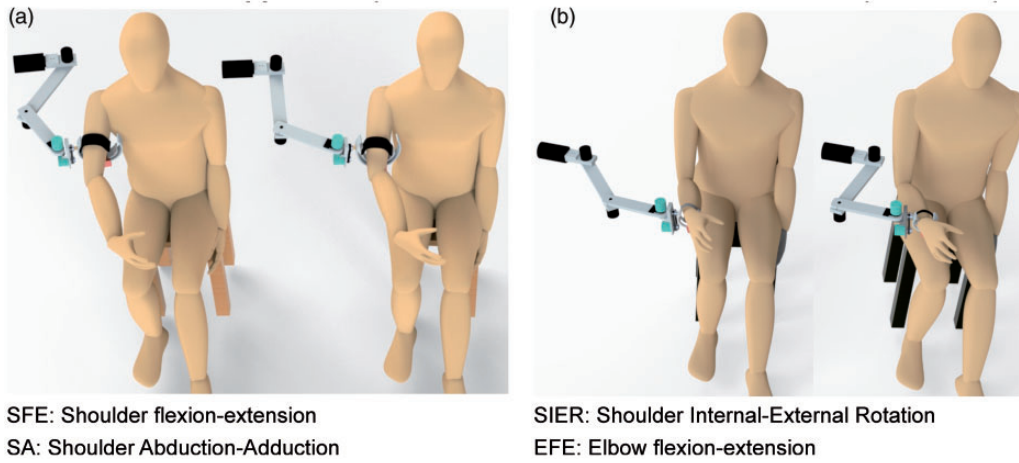


Figure 7. CAD models of a realization of AREBO and the depiction of its use for assisting the different movements of individual joints. (a) When connected to the upper-arm, the robot can assist shoulder flexion/extension and shoulder abduction/adduction by applying forces orthogonal to the upper-arm. (b) When it is connected to the forearm, SIER and EFE can be assisted by applying forces orthogonal to the forearm. It should be noted that this approach for assisting SIER is safer and more comfortable than by providing tangential forces on the upper-arm.¹⁸ The two CAD models in (a) and (b) demonstrate the relative freedom a participant has in sitting with respect to the robot.

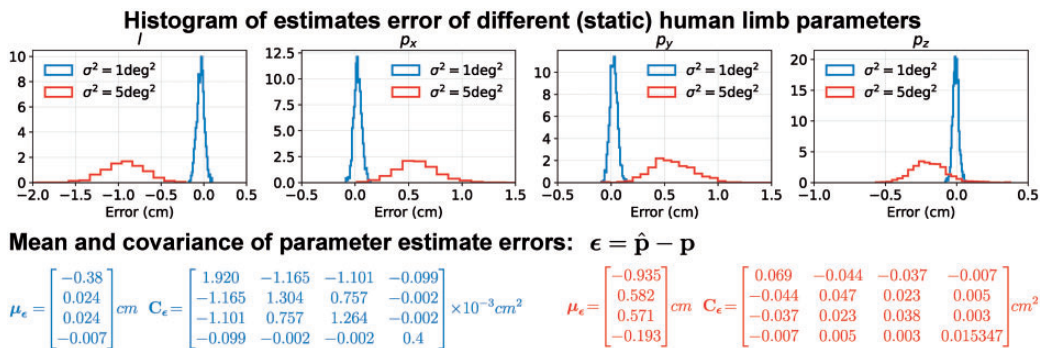


Figure 8. Errors in human limb parameter estimates for two different measurement noise $\sigma^2 = 1 \text{ deg}^2$ and $\sigma^2 = 5 \text{ deg}^2$. The mean and the covariance of the different parameter estimates are shown below the histograms. The text in blue color corresponds to $\sigma^2 = 1 \text{ deg}^2$, while the one in red corresponds to $\sigma^2 = 5 \text{ deg}^2$.

The true value of the parameters is \mathbf{p} , the estimated parameter is $\hat{\mathbf{p}}$, and estimation error ϵ , its mean $\boldsymbol{\mu}_\epsilon$ and covariance \mathbf{C}_ϵ are given by,

$$\epsilon = \hat{\mathbf{p}} - \mathbf{p} = \begin{bmatrix} \hat{l} - l \\ \hat{p}_x - p_x \\ \hat{p}_y - p_y \\ \hat{p}_z - p_z \end{bmatrix}, \quad \boldsymbol{\mu}_\epsilon = \mathbb{E}(\epsilon),$$

$$\mathbf{C}_\epsilon = \mathbb{E}(\epsilon\epsilon^\top) - \boldsymbol{\mu}_\epsilon\boldsymbol{\mu}_\epsilon^\top$$

where, \mathbb{E} is the expectation operator.

Figure 8 shows histograms of the estimation error in the different parameter estimates for two different noise levels in the joint angle measurements. As expected, lower measurement noise results in estimates with smaller bias and variance. The sample mean and covariance of estimation errors are shown below the plots in Figure 8 for both noise variances. The limb length has the largest absolute bias and variance among the four parameters, and also appears to be underestimated for both levels of measurement noise. The parameter p_z has the lowest absolute bias and variance, which also appears to be underestimated. The other two parameters p_x and p_y have intermediate bias and variances, and these are overestimated. p_z is least correlated to the other parameters. The other three parameters appear to be slightly correlated.

Discussion

The paper presented the kinematic design of a 6-*dof* robot – AREBO – capable of assisting movements of individual human joints. The proposed design can assist up to two *dof* of a human joint while ensuring the safe application of assistive forces on the human limb. The optimization of the robot's link lengths, maximizing an objective function consisting of the human limb's workspace and the robot's ability to apply forces in safe directions, was presented. The paper also presented a simple algorithm for continuously estimating the kinematic parameters of the human limb using the joint angles of the robot and the human limb.

Based on the existing evidence and further assuming that robot-assisted therapy is as effective as dose-matched conventional therapy, the ultimate goal of rehabilitation robots is to deliver substantial doses of intense therapy at a small cost to the healthcare system. Realizing this goal requires compact, cost-effective devices that can be easily deployed even in space-constrained healthcare settings and patients' homes while offering superior benefit-to-cost ratio to the user. AREBO presents a minimalistic solution for an arm robot by using three actuated and three passive

dof, while offering several useful features that boost its potential for clinical adoption.

1. AREBO has a very compact and portable structure making it suitable for small clinics and even patients' homes.
2. The reduced number of actuators also makes the overall bill of materials low compared to that of a fully actuated robot.
3. Many recent work targeting robotic mechanisms for the shoulder joint have relied on clever design with active control to ensure suitable alignment to the shoulder joint axes.^{12,13,19,20} From the perspective of assisting just two *dof* of the human limb, AREBO's self-aligning passive joints remove the need for active alignment, thus simplifying the control of the human-robot interaction.
4. The end-effector design of the robot's structure allows it to be used for both the left and right arms without any change in its structure. Without such a feature, a clinic would require dedicated devices for the left and right arms, which is an undesirable solution.
5. The robot can be used for training one or two *dof* at either the shoulder or the elbow, as shown in Figure 7. Shoulder flexion/extension and shoulder abduction/adduction can be trained with the design shown in Figure 7(a). It should be noted that even though we can only train shoulder flexion/extension or abduction/adduction when the robot is connected to the upper-arm (Figure 7(a)), it does not restrict internal/external shoulder rotation movements. A participant can still make unassisted internal/external shoulder rotations while still connected to the robot, which is ensured by the three passive *dof* of the robot. Assisted training of the shoulder internal/external rotation *dof* can be done by connecting the robot to the forearm (Figure 7(b)), which can also be coupled with the elbow flexion-extension. It would be safer and more comfortable to carry out assisted shoulder internal-external rotation by applying forces on the forearm.¹⁸

Another important feature of AREBO is the relaxed constraint on the patient's relative position with respect to the robot. This feature is of significant practical value, as this has the potential to drastically reduce setup time for patients with more severe impairments or in a wheelchair. This ease in setting up the device translates to improved usability and can save time for the clinician when using the robot with multiple patients during a day. This reduced constraint in seating the patient and variations in human limb size between patients result in variations in the human limb's workspace that can be supported by the robot,

and also its manipulability. However, as long as these parameters are within a reasonable range specified in Table 1, the robot with optimized link lengths has an excellent workspace and a good manipulability. The optimized robot can cover, on average, 80% of the human limb's workspace, and for about 60-70% of the points in the robot's joint space, it is "easier" to apply a force orthogonal to the human limb.

The proposed algorithm for human limb parameter estimation allows AREBO to automatically estimate the location of the human joint with respect to the robot, and the length of the human limb, both of which are required for the complete specification of the human-robot closed kinematic chain. This can be done with a short calibration procedure (5 s long). The current results show that with the level of noise expected from rotary sensors, the human limb parameters can be estimated with relatively small bias and variance. There has been prior work on estimating human limb posture when connected to an exoskeleton robot,²¹ and to plan the robot's trajectory for a given human limb trajectory.¹⁸ However, the authors are unaware of any prior work on estimating the location of the human joint and limb length using the human and robot joint kinematic data. One of the assumptions made by the proposed algorithm is that the human limb parameters are fixed over time. It is reasonable to assume that limb length does not change over time, but the same cannot be assumed about the limb's location. For example, when the robot is connected to the upper-arm (as shown in Figure 7(a)), trunk or scapular movements will result in the translation of the glenohumeral joint. Thus, it would be ideal if the estimation can be implemented using data from the recent past in a recursive form with the following assumptions:

1. Human limb length does not undergo any change over time.
2. The location of the human limb does not undergo a drastic change in the window of data used for the estimation process.

Based on these assumptions, the recursive estimate at time n can be posed as multiple objective minimization problem,

$$\hat{\mathbf{v}}_n = \arg \min_{\mathbf{v}_n} \|\mathbf{A}\mathbf{v}_n - \tilde{\mathbf{b}}\|_2^2 + \lambda \|\mathbf{W} \cdot (\mathbf{v}_n - \hat{\mathbf{v}}_{n-1})\|_2^2,$$

$$0 < \lambda \in \mathbb{R}$$

where, $\hat{\mathbf{v}}_n, \hat{\mathbf{v}}_{n-1}$ are the parameter estimated at time n and $n - 1$, respectively. \mathbf{W} is a weight matrix that assigns different weights for change in different

parameters (e.g., the weight for a change in l can be set much higher than the other parameters). The ability to track changes in human limb parameters can allow the robot to automatically detect compensatory movements within and across sessions, which can be a useful measure of motor ability.²² Given the stochastic nature of the estimates of the human limb parameters, large errors in their estimate can have implications to the safety of the human-robot interaction. Any errors in the human limb parameters will lead to errors in the planning of movement trajectories of the human-robot closed chain. However, these issues can be minimized or even prevented by ensuring that the human limb is never moved out of a pre-set (safe) joint range of motion, and by never applying inappropriately directed or large magnitude interaction forces, all of which can be ensured by the sensors available on the robot. Inappropriate values from these sensors can be used to trigger the necessary safety mechanisms in the robot to ensure the safety of the participant.

We finally point out the limitation of AREBO's simplicity gained at the expense of training coordinated multi-joint movements, i.e. the inability to perform assisted training of multi-joint movements possible with exoskeleton robots such as BONES,¹⁰ ArmIn,⁸ etc. From the neurorehabilitation perspective, the current evidence indicates that simple single-joint training is as effective as complex multi-joint training.⁴ The study by Milot et al. showed that both single and multi-joint training with BONES resulted in improvements in both sensorimotor impairments and function.⁴ About 75% of the participants in this study had an equal preference for both single-joint and multi-joint training with the robot.⁴ There is also evidence for the transfer of training effects to untrained ADL,⁵ which can be extrapolated to the possibility of single-joint training generalizing to complex multi-joint movements. Furthermore, single-joint exercises are an important component of training protocols in patients with severe sensorimotor impairments in impairment oriented training.^{23,24} These studies and the practical advantages of AREBO make a strong case for developing and evaluating the clinical usability and efficacy of such simple, compact robots for arm neurorehabilitation. If found to be therapeutically effective, such robots have the best potential for clinical translation and widespread adoption.

Conclusion

The paper presented the kinematic design and optimization of a compact 6-*dof* robot for individual joint training of the human arm. The proposed robot uses three actuated *dof* and three passive self-aligning *dof* keeping the overall structure of the robot simple and

cost-effective. The proposed robot allows significant freedom in terms of the seating of a patient with respect to the robot, can easily accommodate arms of different sizes, and can be used for both the left and right arms without any change to its structure. The paper also presented an approach for automatically tracking the kinematic parameters of a human limb attached to the robot, which can be used by a robot controller to impose the desired movements to the human limb.

Declaration of conflicting interests

The author(s) declare no potential conflicts of interest with respect to the research, authorship, and/or publication of this article.

Funding

The author(s) received no financial support for the research, authorship, and/or publication of this article.

Guarantor

Sivakumar Balasubramanian and S Sujatha.

Contributorship

SB, SG, and SS conceived the initial ideas for the robot and its design. SG and SB explored various potential designs for the robot. SB carried out the optimization of the robot link lengths. SB, SG, and JSM worked on the estimation algorithm and its evaluation through simulated data. SB prepared the first draft of the manuscript with help from SG and JSM. All authors reviewed the manuscript. SB and SS oversaw the activities of the project.

Acknowledgements

The authors thank Mr. Aravind Nehrujee, Mr. Samuel Elias, and Mr. Sathish Balaraman for their help in building and rendering the 3D models for the robot.

ORCID iDs

Sivakumar Balasubramanian  <https://orcid.org/0000-0001-5915-1346>

Javeed Shaikh Mohammed  <https://orcid.org/0000-0001-9079-3101>

Note

- I. A *kinematic chain* is an assembly of rigid bodies that are interconnected through a set of joints to allow constrained movements with respect to each other. A *closed* kinematic chain is one that forms loops and every link is connected through two joints to two adjacent links.

References

1. Prange GB, Jannink MJA, Groothuis-Oudshoorn CGM, et al. Systematic review of the effect of robot-aided therapy on recovery of the hemiparetic arm after stroke. *Jrrd* 2006; 43: 171–184.
2. Kwakkel G, Kollen BJ and Krebs HI. Effects of robot-assisted therapy on upper limb recovery after stroke: a systematic review. *Neurorehab Neural Repair* 2008; 22: 111–121.
3. Lo AC, Guarino PD, Richards LG, et al. Robot-assisted therapy for long-term upper-limb impairment after stroke. *N Engl J Med* 2010; 362: 1772–1783.
4. Milot M-H, Spencer SJ, Chan V, et al. Crossover pilot study evaluating the functional outcomes of two different types of robotic movement training in chronic stroke survivors using the arm exoskeleton bones. *J Neuroeng Rehab* 2013; 10: 112.
5. Schaefer SY, Patterson CB and Lang CE. Transfer of training between distinct motor tasks after stroke: implications for task-specific approaches to upper-extremity neurorehabilitation. *Neurorehab Neural Repair* 2013; 27: 602–612.
6. Fluet GG, Merians AS, Qiu Q, et al. Comparing integrated training of the hand and arm with isolated training of the same effectors in persons with stroke using haptically rendered virtual environments, a randomized clinical trial. *J Neuroeng Rehab* 2014; 11: 126.
7. Klein J, Spencer SJ and Reinkensmeyer DJ. Breaking it down is better: haptic decomposition of complex movements aids in robot-assisted motor learning. *IEEE Trans Neural Syst Rehab Eng* 2012; 20: 268–275.
8. Nef T, Guidali M and Riener R. Armin iii—arm therapy exoskeleton with an ergonomic shoulder actuation. *Appl Bionics Biomech* 2009; 6: 127–142.
9. Sanchez RJ, Wolbrecht E, et al. R, Smith, J, Liu, S, Rao. A pneumatic robot for re-training arm movement after stroke: rationale and mechanical design. In: *9th international conference on rehabilitation robotics*. New York: IEEE, 2005, pp.500–504.
10. Klein J, Spencer SJ, Allington J, et al. Biomimetic orthosis for the neurorehabilitation of the elbow and shoulder (bones). In: *2008 2nd IEEE RAS & EMBS international conference on biomedical robotics and biomechanics*. New York: IEEE, 2008, pp.535–541.
11. Trigili E, Crea S, Moise M, et al. Design and experimental characterization of a shoulder-elbow exoskeleton with compliant joints for post-stroke rehabilitation. *IEEE/ASME Trans Mechatron* 2019; 24: 1485–1496.
12. Yves Z, Alessandro F, Robert R, et al. Anyexo: a versatile and dynamic upper-limb rehabilitation robot. *IEEE Rob Autom Lett* 2019; 4: 3649–3656.
13. Bongsu K and Deshpande AD. An upper-body rehabilitation exoskeleton harmony with an anatomical shoulder mechanism: design, modeling, control, and performance evaluation. *Int J Rob Res* 2017; 36: 414–435.
14. Krebs HI, Hogan N, Aisen ML, et al. Robot-aided neurorehabilitation. *IEEE Trans Rehab Eng* 1998; 6: 75–87.
15. Campolo D, Tommasino P, Gamage K, et al. Lorenzo masia. H-man: a planar, h-shape cabled differential robotic manipulandum for experiments on human motor control. *J Neurosci Meth* 2014; 235: 285–297.

16. Che FY, Alejandro M-C, Roger G, et al. *IEEE/RSJ international conference on intelligent robots and systems*. New York: IEEE, 2009, pp.4080–4085.
17. Rosati G, Gallina P and Masiero S. Design, implementation and clinical tests of a wire-based robot for neuro-rehabilitation. *IEEE Trans Neural Syst Rehab Eng* 2007; 15: 560–569.
18. Jarrassé N and Morel G. Connecting a human limb to an exoskeleton. *IEEE Trans Robot* 2012; 28: 697–709.
19. Christensen S and Bai S. Kinematic analysis and design of a novel shoulder exoskeleton using a double parallel-ogram linkage. *J Mech Rob* 2018; 10: 041008.
20. Hunt J, Lee H and Artemiadis P. A novel shoulder exoskeleton robot using parallel actuation and a passive slip interface. *J Mech Rob* 2017; 9: 011002.
21. Cortés C, Ardanza A, Molina-Rueda F, et al. Upper limb posture estimation in robotic and virtual reality-based rehabilitation. *BioMed Res Int* 2014.
22. Cirstea MC and Levin MF. Compensatory strategies for reaching in stroke. *Brain* 2000; 123: 940–953.
23. Platz T. Impairment-oriented training (iot)—scientific concept and evidence-based treatment strategies. *Restorai Neurol Neurosci* 2004; 22: 301–315.
24. Thomas P, Stefanie v. K, Jan M, et al. Best conventional therapy versus modular impairment-oriented training for arm paresis after stroke: a single-blind, multicenter randomized controlled trial. *Neurorehabil Neural Repair* 2009; 23: 706–716.